Structural Heterogeneity and Its Influence on Non-linear Deformation and Fracture of Ultra-soft Hydrogels

Yuanyuan Wei, Donghao Zhao, Costantino Creton, Tetsuharu Narita

Macromolecules 2023 ma-2023-01581p

Structural Heterogeneity and Its Influence on Non-linear Deformation and Fracture of Ultra-soft Hydrogels

Yuanyuan Wei, Donghao Zhao, Costantino Creton, Tetsuharu Narita**

Laboratoire Sciences et Ingénierie de la Matière Molle, CNRS UMR 7615, ESPCI Paris, Sorbonne Université, PSL Université, 75005 Paris, France

costantino.creton@espci.fr, tetsuharu.narita@espci.fr

Abstract

Understanding the deformation and fracture behavior of human organs exhibiting a very low stiffness (< 1 kPa) is of vital importance to gain information on how these soft tissues react on the medical device during loading conditions in surgical robotics applications. We investigated the deformation and fracture behavior of model poly(vinyl alcohol) ultra-soft hydrogels by puncture tests with flat-ended indenters whose size is comparable to the elasto-capillary length, with a particular focus on the effect of structural heterogeneity. By tuning the polymer and cross-linker concentrations, gels with modulus ranging from 56 – 2700 Pa were synthesized having varied structural heterogeneity, examined by light scattering. We found that structural heterogeneity plays a key role in lowering the fracture resistance of the soft gels under large non-linear deformation. This work provides insights into the mechanics and fracture of ultra-soft materials under extreme deformation conditions and opens the question of the interplay between elasticity and capillarity in such ultra-soft gels at small length scales.

KEYWORDS: Puncture, Fracture, deformation, ultra-soft hydrogel, structural heterogeneity.

TOC graphic

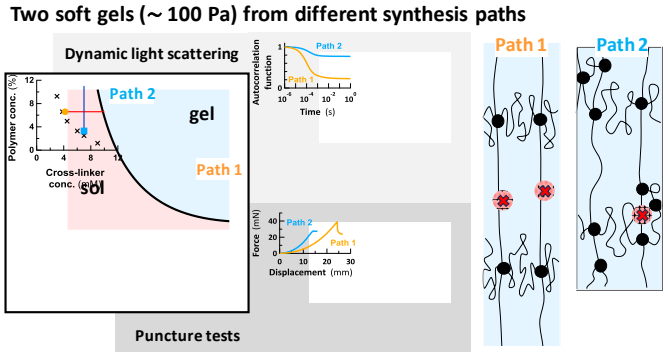

Introduction

Hydrogels are networks of cross-linked polymer chains swollen in water. Thanks to their high water contents and biocompatibility, hydrogels are good candidates for biomedical applications such as tissue engineering, artificial cartilage, vessels, prosthetic joints, soft contact lenses, etc[1]. The growing demand for hydrogels highlights the importance of understanding their mechanical properties, especially fracture resistance properties for stress-bearing applications. Many types of tough hydrogels have been extensively investigated recently, either for covalently cross-linked[2, 3], physically cross-linked[4,5], or double network hydrogel,[6] and several different mechanisms to prevent crack initiation and/or crack propagation have been proposed[7,8]. These tough hydrogels have a modulus typically on the order of tens of kPa, while some of the human organs (brain, breast, and lung) exhibit a very low stiffness, with a modulus as low as tens of Pa. Understanding the deformation and fracture behavior of such ultrasoft solids, or how soft tissues react to a medical device during loading conditions, is of practical and academic importance, given the notable advances in medical robotics and surgical tactile sensors application.[9,10]

When investigating the fracture behavior of soft solids, elasto-capillarity needs to be considered. The elasto-capillary length, l_{ec}, defined as the ratio between surface tension and modulus, indicates the length scale over which the capillary effect is dominant. For some materials with an extremely large modulus, such as metals with moduli ~ 100 GPa, the effect of surface tension is insignificant and can be ignored as the l_{ec} is infinitely small. For soft elastic materials with a modulus in the order of 10 – 100 kPa, the value of l_{ec} can be micrometric, and it has been reported that the surface tension can cause shape changes in soft solids, such as the flattening of

a sharp corner or the closing of a crack inflated by hydrostatic pressure[11-13]. Hui et al.[14] demonstrated that surface tension could mitigate crack growth by lowering the applied energy release rate $\mathcal{G}$. Various mechanisms of capillarity-induced deformation have been reported in the last 10 years. For the ultrasoft solids having $G' \sim 10$ Pa, l_{ec} can be on the order of 1 mm, approaching the sample size. In this case, surface tension does play a significant role in the mechanical properties. In this work, we studied the fracture behaviors of model ultrasoft hydrogels.

The challenges of performing fracture tests of ultrasoft hydrogels, with $G' < 1$ kPa lie in two aspects. First, the ultrasoft nature of the sample makes it difficult to manipulate and perform mechanical tests since the sample might not even support its weight under the influence of gravity in a specific dimension.[15] Conventional fracture characterization tests, such as a pure shear test commonly used for harder hydrogels are difficult to apply, and an appropriate geometry/technique for the fracture measurements of hydrogels is necessary. Second, while the modulus of these hydrogels can easily be controlled by changing either the polymer concentration or the cross-linker concentration, the resulting network structure can be quite different depending on the synthesis conditions and could influence the nonlinear mechanical and fracture properties. This aspect has rarely been discussed in the literature and is the focus of this paper.

Puncture experiments are promising mechanical tests to detect the large local deformation and failure in ultrasoft solids.[16] This technique involves inserting a long and sharp indenter into the soft material and recording the puncture force as a function of the indenter displacement during

the puncture process. The point where the puncture force sharply drops corresponds to the failure of the material, where the indenter pierces the sample's surface. Puncture tests have been recently used to characterize the fracture behavior of acrylic triblock copolymer gels with a modulus above several kPa.[17-19] Fakhouri et al. investigated the puncture process to failure and revealed two failure regimes by applying a process zone model of fracture: stress-limited and energy-limited[18]. Rattan and Crosby investigated the effect of polymer volume fraction on fracture initiation in the acrylic triblock copolymer gels over length scales around the elasto-capillary length.[17] The length scale of the measurements was tuned either by varying the size of the spherical-tipped indenter (0.4 – 66 μm), or by varying the modulus of the gels (2.7 – 54 kPa, with l_{ec} ranging between 0.2 and 3.4 μm). To the best of the authors' knowledge, a systematic study of the fracture properties of ultrasoft solids by puncture tests at the length scale below the elasto-capillary length has not been reported.

For ultrasoft gels, their macroscopic properties are remarkably impacted by network structure heterogeneity. There are generally three types of heterogeneity in polymer networks:[20] (1) structural heterogeneities stemming from the inhomogeneous spatial distribution of cross-links and (2) topological defects including dangling chain ends, loops, etc. (3) connectivity heterogeneity. When the polymer concentration or cross-linker concentration is decreased to lower the modulus of the network, these different types of heterogeneities can evolve depending on the synthesis conditions. An inhomogeneous network is expected to give rise to localized stresses on certain chemical bonds at the molecular level and to facilitate the initiation of larger defects that can propagate into cracks.[21] However, the impact of structural heterogeneity on the

linear elasticity as well as the nonlinear fracture behavior of ultrasoft hydrogels remains unexplored.

This paper focuses on the effect of the structural heterogeneity of poly (vinyl alcohol) (PVA) hydrogels on their deformation and fracture behavior. The differences in structural heterogeneity of the gels prepared from two different synthesis paths were first elucidated by dynamic light scattering (DLS). Then, puncture experiments were used to characterize the deformability and fracture resistance of gels with a comparable linear elastic modulus (elasticity), but with a distinct structural heterogeneity at the elasto-capillary length scale.

Experimental Section

Materials. Poly(vinyl alcohol) (PVA) with a degree of hydrolysis: 88 mol% and molecular weight 67,000 g/mol, glutaraldehyde (GA, 25 wt% aqueous solution), and hydrochloric acid (HCl) were purchased from Sigma-Aldrich and used as received.

Gels Preparation. A PVA stock solution at a concentration of 13.2 wt% (or 3 M for the repeating unit) was prepared by dissolving the PVA powder in deionized water at 95 ℃ and stirring vigorously over 4 h. Chemically cross-linked PVA hydrogels were prepared by cross-linking PVA with the cross-linker GA in the presence of HCl (0.05 M). In order to vary the elastic modulus and structure, the PVA and GA concentrations were systematically varied by following two paths. In Path 1, the PVA concentration was set to 6.6 wt% (or 1.5 M for the repeating unit), and the GA concentration was varied between 4 and 10 mM. In Path 2, the PVA concentration was varied from 3.3 to 11 wt% (or 0.75 – 2.5 M) at a fixed GA concentration of 7 mM. For puncture measurements, the system was gelled in a cylindrical glass vial with a diameter of 25 mm. For dynamic light scattering measurements the samples were prepared in a glass tube (10 mm in diameter) with a pregel solution volume of 5 mL. A syringe filter of 0.22 μm was used to prefilter the pregel solution. We allowed the cross-linking reaction to run for at least 12 h.

Rheology. Rheological measurements were carried out on an ARES strain-controlled rheometer (TA Instruments, USA) with a steel cone-plate geometry (25 mm in diameter, 0.053 mm in the gap) and a roughened surface. A fresh pregel mixture solution was loaded for a time sweep measurement to track the gelation behavior of the PVA sample. A frequency sweep test with an

angular frequency range of 0.1 – 100 rad/s at a linear strain of 2 % was performed, followed by a strain sweep with amplitude ranging from 0.1 – 1000 % at a fixed frequency of 1 Hz. For each measurement, the exposed surface of the sample was covered with a thin layer of low-viscosity silicone oil to avoid water evaporation.

Dynamic light scattering (DLS). DLS was performed with an ALV CGS-3 goniometer system (ALV, Langen, Germany), equipped with a cuvette rotation/translation unit CRTU and a He-Ne laser (22 mW at λ = 632.8 nm). It is known that the dynamic light scattering signals from chemically cross-linked hydrogels are nonergodic, and in order to accurately take into account the position-dependent concentration gradient (spatial heterogeneity), an ensemble averaging is necessary. The ensemble-averaged autocorrelation function of the scattered light intensity was measured by vertically translating the sample at a constant rate, during time-averaging.

Puncture. Puncture tests were performed on a custom apparatus consisting of a motorized stage, flat-ended indenter, force sensor, and camera. A balance with a precision of 0.1 mg was placed at the bottom of the sample and used as a force sensor to measure the puncture loading force. As indenters, flat-end metal needles (obtained from Hamilton Company, Reno, NV) with a radius of 0.13 – 0.31 mm were used. They were backfilled with epoxy and fixed to the adapter in the actuator (motorized stage). The insertion velocity of the indenter was set to 0.25 mm/s in this study. The displacement and loading force as a function of time were recorded during the puncture process, and the camera captured the corresponding images.

Results and Discussion

Sol-Gel Phase Diagram.

Figure 1 shows the gelation phase diagram of the PVA hydrogels. The black solid curve indicates the gelation limit of PVA, determined by the so-called "tilting-a-tube" method,[22] or observation of the flowability of the inverted sample in a small vial. Below this gelation limit line, the system is in a liquid state with either a low cross-linker concentration or a low polymer fraction. Above that, the system demonstrates solid-like behavior.

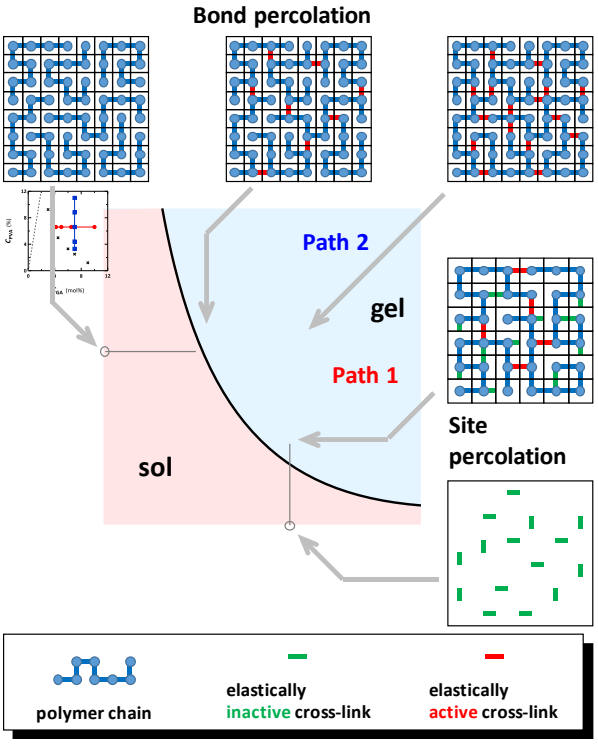

Figure 1. Experimental sol-gel phase diagram of the PVA hydrogels shows the two measurement paths (Path 1 and Path 2) used in this work. The gray dashed line indicates two cross-linkers per polymer chain. The five schematics with grids describe network structure based on bond percolation and site percolation theory.

For the gel system shown in **Figure 1**, we studied two different gelation paths to investigate the role played by the network architecture in the dynamic, deformation, and fracture properties of the gels with varied values of the elastic modulus. In Path 1, at a fixed polymer concentration (C_{PVA} = 6.6 wt%) the cross-linker concentration was varied from 4 to 10 mM (horizontal red line and circles). In Path 2, a similar modulus range was obtained by changing the polymer concentration C_{PVA} from 3.3 to 8.8 wt% (or 0.75 to 2.5 M in repeating unit molar concentration) at a constant GA concentration (C_{GA} = 7 mM) (vertical blue line and squares). From the rheology test (**Figure S1**), we confirmed that the viscous modulus *G*" is far lower than the elastic modulus *G*' which is little dependent on frequency, indicating that the chemically cross-linked gel system can be considered purely elastic with a negligible viscous component. Path 1 corresponds to the so-called gelling by "bond percolation" situation, where there are sufficient binding sites to cross-link (here diols on PVA chains), and the distance from the percolation points is determined by the probability of bond formation, or by the concentration of bonds (cross-links, adjusted by the GA concentration). Path 2 corresponds to the "site percolation" situation, where with a sufficient bond formation probability, the site probability (concentration of the sites, here PVA concentration) determines the distance from the percolation point.[20,23] It should be noted that gels close to the site percolation limit (soft gels from Path 2) can contain a large number of elastically inactive cross-links, which could cause spatial heterogeneity of the network.

In **Table 1**, we summarize the synthesis conditions (C_{PVA} and C_{GA}) of the PVA chemical gels studied in this work. The value of the modulus *G*' is also shown. For the gels from Path 1, we have *G*' = 56 – 1700 Pa, and for those from Path 2, we have 130 – 2700 Pa. The mesh size of the network, defined as $\xi \sim (k_B T/G')^{1/3}$, with the thermal energy $k_B T$, is calculated and listed in the

table. We calculate the elasto-capillary length l_{ec} according to the gel modulus, $l_{ec}= \gamma/G'$, where γ is the surface tension of the gel. It should be noted that we used the value of 6.6 wt% PVA solution (γ = 52 mN/m) measured by a tensiometer, as we were not able to measure the surface tension of the hydrogels. The PVA is surface active and the surface tension of aqueous solutions does not depend on the concentration above 1 %.[24,25] Thus we assumed that the surface tension of the PVA hydrogels studied in this work was close to 52 mN/m. For the gels from Path 1, the value of l_{ec} ranges from 911 to 30 μm, and for those from Path 2, that value ranges from 392 to 19 μm. The needle size for the puncture measurements, used as characteristic length of the measurements, ranges from 130 to 310 μm. This value is comparable to that of l_{ec}.

Table 1. Summary of Modulus and Characteristic Lengths for Gels from Path 1 and Path 2.

Path	C_{PVA} (wt %)	C_{GA} (mM)	G' (Pa)	$\xi_{mesh}\sim(k_BT/G')^{1/3}$ (nm)	$l_{ec}=\gamma/G'$ (μm)	ξ_c (nm)
1	6.6	4.2	56	41.8	911	7.0
		4.5	110	33.4	464	/
		5	250	25.4	204	6.6
		6.5	560	19.4	91	/
		7	800	17.2	64	5.4
		10	1700	13.4	30	5.1
2	3.3	7	130	31.6	392	6.9
	4.4		210	26.9	243	6.3
	6.6		800	17.2	64	5.4
	8.8		1400	14.3	36	/
	11		2700	11.5	19	5.6

Structure Heterogeneity Htudied by DLS.

To illustrate the structural architecture of the PVA gels synthesized from two different experimental paths with a comparable modulus, we performed DLS measurements. The normalized ensemble-averaged field autocorrelation functions $g^{(1)}$ are plotted as a function of time for the PVA gels made from Path 1 and Path 2 in **Figure 2**. The autocorrelation function of these gels is typical for chemical gels, exhibiting a relaxation mode, and a long-time plateau, and one can characterize the dynamics by two characteristics: the relaxation time and the plateau amplitude. Below we discuss the modulus dependence of these two characteristic values to evaluate the dynamics and structure of the gels.

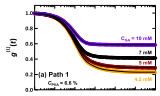

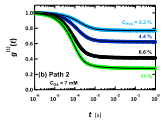

Figure 2. Normalized ensemble-averaged field autocorrelation function $g^{(1)}$ measured at an angle of 90°, for the PVA gels made from Path 1 (a) and from Path 2 (b).

Gel Mode Dynamics

For all the gels tested, one can see a characteristic decorrelation occurring at about 10^{-4} s. This fast decorrelation is the so-called gel mode, which is linked to the collective motion of polymer chains in the network.[26] Generally, this is the only relaxation mode observed in a chemical gel. In order to roughly estimate the distribution of the characteristic times, we used CONTIN, and the results are shown in **Figure S2**. One can clearly see a large peak at about 10^{-4} s for all the samples. For Path 1 (constant polymer concentration, varying cross-linker concentration), the position and the width of this large peak do not depend on the cross-linker concentration (thus do not depend on the modulus), while for Path 2 (constant cross-linker concentration, varied polymer concentration), the peak shifts to longer times and its width increases, with *decreasing* polymer concentration (thus with decreasing modulus). Apart from this dominant peak, one also finds smaller peaks. CONTIN is sensitive to measurement noises which can result in false peaks, still, we can consider two smaller peaks, one at about 10^{-3} and the other at about 10^{-2} s, which are systematically detected. These smaller peaks become less pronounced with an increase in the modulus of the gels.

In order to evaluate the dynamics as quantitatively as possible, the normalized field autocorrelation function of the gel is fitted with the following three-component stretched exponential function,

$$g^{(1)}(t) = A_1 exp\left[-\left(\frac{t}{\tau_1}\right)^{\alpha_1}\right] + A_2 exp\left[-\left(\frac{t}{\tau_2}\right)^{\alpha_2}\right] + A_3 exp\left[-\left(\frac{t}{\tau_3}\right)^{\alpha_3}\right] + A_{\text{frozen}} \qquad 1$$

where A is the amplitude of the decorrelation modes, A_{frozen} is the amplitude of the plateau ($A_{\text{frozen}} = 1 - A_1 - A_2 - A_3$), τ is the characteristic time and α is the stretch exponent which represents the distribution of characteristic times around the mean value τ. The subscripts 1, 2 and 3 correspond to the three dynamic modes. This equation fits well with the experimental data for all the gels tested, as shown in **Figure 2** (solid curves).

The nature of the dynamic modes can be analyzed by their scattering vector dependence. We confirmed that τ_1 scales with the scattering vector q as $\tau_1 \sim q^{-2}$, as expected for the gel mode which is diffusive. As an example, the result of the gel with C_{PVA} = 6.6 wt% and C_{GA} =7 mM (black symbols which are found in both Path 1 and 2) is shown in **Figure S3**. For the two slower modes having a low amplitude, the exponent varies between –1.1 and –2.2. In general, it is difficult to determine the origin of slow modes in gels, especially when their amplitude is small. Thus, in this work, we do not further characterize them, and focus only on the fast and dominant mode.

The gel mode is further characterized to correlate the obtained best fitting parameters with the polymer and cross-linker concentrations. Since the gel mode characteristic time τ_1 scales with q as $\tau_1 \sim q^{-2}$, the apparent collective diffusion coefficient is calculated as $D_A = \frac{1}{\tau_1 q^2}$. It should be noted that in a nonergodic medium, the heterodyne approach allows us to better evaluate the dynamics.[20,27] The decorrelation observed in the autocorrelation function consists of the

homodyne component (correlation of the intensity from the fluctuating gel mode component) and of the heterodyne component (correlation between the intensity from the fluctuating component and that from the nonfluctuating frozen-in component). The true collective diffusion coefficient D can be determined as $D = D_A(2 - X)$, where X is the ratio of the average scattered light intensity from the fluctuating gel mode to the total intensity, $X = \langle I_{gel} \rangle / \langle I_{total} \rangle$.

The characteristic length scale of the gel mode, correlation length, is calculated from the Stokes-Einstein relation as $\xi_c = k_B T/(6\pi\eta_s D)$, where η_s is the viscosity of the solvent (water). In **Figure 3a** and **3b** the correlation length ξ_c was plotted against cross-linker concentration C_{GA} (for Path 1) and against polymer concentration C_{PVA} (for Path 2). As seen in **Figure 3a**, the value of ξ_c for the gel from Path 1 does not exhibit a strong cross-linker concentration dependence, and is found to be about 7.0 – 5.1 nm. This value is slightly lower than that measured for the solution of the same PVA concentration (7.5 nm, open diamond). This scattering correlation length is shorter than the mesh size of the network estimated from the modulus as $\xi_{mesh} = (k_B T/G')^{1/3}$, which is found to vary between 13 and 42 nm for these gels made from Path 1. **Figure 3b** shows the PVA concentration dependence of ξ_c for the PVA gels from Path 2 and for solutions. In solution, ξ_c does not show a strong polymer concentration dependence, ranging from 6.7 to 7.7 nm. In the gels the value of ξ_c is comparable to that of the solution ranging from 5.4 to 6.9 nm. For these gels from Path 2, the value of the mesh size (determined from the modulus) varies between 12 and 32 nm. The gels synthesized from the two synthetic paths are compared by plotting the correlation length as a function of the modulus (**Figure 3c**). The value of ξ_c is not dependent on the synthetic path. This result indicates that the gel mode dynamics are not

strongly influenced by the structure, since they are averaged over the sample positions, in a similar manner as the linear elastic modulus.

Figure 3. Correlation length ξ_c of PVA gels and solutions. (a) ξ_c versus GA concentration for gels made from Path 1 and PVA solution at C_{PVA} = 6.6 wt%. (b) ξ_c versus PVA concentration for gels made from Path 2 and solutions. (c) ξ_c versus gel modulus.

Frozen-In Structure (Static Light Scattering)

The fact that the autocorrelation function does not fully decorrelate to zero but shows a plateau indicates that a part of the scattered light intensity does not fluctuate with time. This unfluctuating part is attributed to the spatially frozen concentration gradient in the polymer network: permanent cross-links induce a static concentration gradient and light scattering from this spatial heterogeneity does not fluctuate. From the normalized field autocorrelation function of the gels from Path 1 and 2 shown in **Figure 2** the amplitude of the plateau A_{frozen} is estimated

and plotted as a function of modulus in **Figure 4a**. For the gels from Path 1 (constant polymer concentration, varied cross-linker concentration), the value of A_{frozen} *increases* with increasing modulus (thus with cross-linker concentration), while in Path 2 (constant cross-linker concentration, varied polymer concentration), it *decreases* with increasing modulus (thus with polymer concentration).

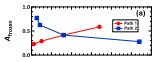

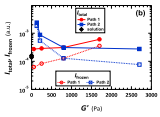

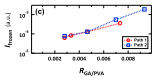

Figure 4. (a) Amplitude of the plateau A_{frozen} in normalized field autocorrelation function versus modulus. (b) Scattered light intensity I_{total} (filled symbols, solid lines) and frozen-in intensity I_{frozen} (open symbols, dashed lines). (c) I_{frozen} as a

function of the cross-linking ratio (molar ratio of GA to diol sites on PVA). θ = 90°.

The scattered light intensity is also sensitive to the network heterogeneity; thus, its modulus dependence is quantitatively studied. The average scattered light intensity I_{total} corresponding to the dynamic measurements in **Figure 2**, is plotted as a function of modulus in **Figure 4b** (filled symbols). The value of I_{total} for the PVA solutions is also plotted at G' = 0 Pa (filled diamonds). For all of the gel samples studied, the scattered light intensity is higher than that for the solutions. For Path 1, the scattered light intensity at a low modulus is almost constant (around 0.0003), and the hardest gel has a slightly higher value (0.0004). For Path 2 I_{total} decreases with increasing modulus. For the softest gel tested, the intensity (0.0024) is 1 order of magnitude higher than that of the soft gels from Path 1. These modulus dependences of the scattered light intensity correspond well to those of the amplitude of the plateau, suggesting the importance to study the intensity of the frozen-in structure.

The contribution of the frozen-in structure to the scattered light intensity, I_{frozen}, can be determined from the total intensity and the amplitude of the plateau in the ensemble averaged normalized *intensity* autocorrelation function $g^{(2)} - 1$. The amplitude of the gel mode consists of the homodyne and heterodyne components $a_{\text{gel}} = X^2 + 2X(1-X)$. The amplitude of the plateau is written as

$$a_{\text{frozen}} = 1 - a_{\text{gel}} = 1 - X^2 - 2X(1-X) = (1-X)^2 \qquad 2$$

From Siegert's relation for the normalized autocorrelation functions, $g^{(2)} - 1 = \left|g^{(1)}\right|^2$, one has $a_{\text{frozen}} = {A_{\text{frozen}}}^2$.

In **Figure 4b**, the value of I_{frozen} is also plotted (open symbols). I_{frozen} exhibits a modulus dependence more pronounced than I_{total}. For Path 1, I_{frozen} exponentially increases with the modulus by one order of magnitude, while for Path 2, a two-order of magnitude decrease is found in the same modulus range. The difference in I_{frozen} between the soft gels from the two paths is remarkable. In **Figure S4**, the scattered light intensity for the fluctuating intensity defined as $I_{\text{gel}} = I_{\text{total}} - I_{\text{frozen}}$ is shown as a function of modulus. For both paths the modulus dependence is weak and the value of I_{gel} varies within a factor of 3.

For this system under the studied conditions, we found a simple relationship between the frozen-in intensity and the cross-linking ratio ($R_{\text{GA/PVA}}$). The value of I_{frozen} exponentially increases with $R_{\text{GA/PVA}}$ and in this representation there is little difference between the gels made from the two paths. This relation could provide us with a parameter to control the spatial heterogeneity. However, the experimentally accessible range of $R_{\text{GA/PVA}}$ is not wide. The lower bound of the cross-linking ratio to prepare soft gels depends on the degree of polymerization of the polymer. The PVA used in this work has a degree of polymerization of about 1400. One can expect that at least 2 cross-linkers per chain are necessary to percolate the network, thus the minimum degree of cross-linking ~ 2/1400 ≈ 0.0014. In **Figure 1**, the gray dashed line corresponds to this limit. At the studied conditions the polymer concentration is not high enough to reach this limit, the lowest value which we experimentally have is 0.0028. There are also upper bounds depending on the path. For Path 2 (constant cross-linker concentration and varied polymer concentration), there

is a minimum polymer concentration to percolate which is expected to be of the order of the overlap concentration of the polymer (~ 1 wt%). Thus polymers with higher degrees of polymerization would be preferable to expand this limit. For Path 1 (constant polymer concentration, varied cross-linker concentration), upon increasing the cross-linker concentration, macroscopic phase separation can occur, or the value of the polymer concentration under preparation conditions is lower than that at equilibrium swelling and the gel shrinks. For Path 1 with C_{PVA} = 6.6 wt%, if C_{GA} > 15 mM ($R_{GA/PVA}$ = 0.01) shrinkage is observed. This macroscopic phase separation is expected to be observed only with neutral polymer gels.

In order to discuss the structural differences between the soft gels from Path 1 and Path 2 as demonstrated by the light scattering measurements, we schematically illustrate their proposed network structure (**Figure 5**). Starting from the gel with C_{PVA} = 6.6 wt% and C_{GA} = 7 mM (**Figure 5b**), which is found in both Path 1 and 2, the modulus can be decreased either by decreasing the cross-linker concentration (Path 1) or by decreasing the polymer concentration (Path 2). The structure of the soft gel made with Path 1 (C_{PVA} = 6.6 wt% and C_{GA} = 4.2 mM) is schematically shown in **Figure 5a**. The correlation length is comparable to that of the gel shown in Figure 5b, while the average mesh size increases as its modulus decreases. Cross-linking locally increases the polymer concentration thus the static heterogeneity increases with the degree of cross-linking, still, in Path 1 the difference is small. The structure of the soft gel in Path 2 (C_{PVA} = 3.3 wt% and C_{GA} = 7 mM) is shown schematically in **Figure 5c**. Compared with the gel in **Figure 5b**, the mesh size increases. In these synthesis conditions where the cross-linking ratio is high, the increase in the polymer concentration in the cross-linked zone further increases the cross-linking reaction rate, resulting in local increase in the polymer concentration,

thus in the unevenly distributed polymer chains and cross-links. This spatial heterogeneity causes an increase in I_{frozen}.

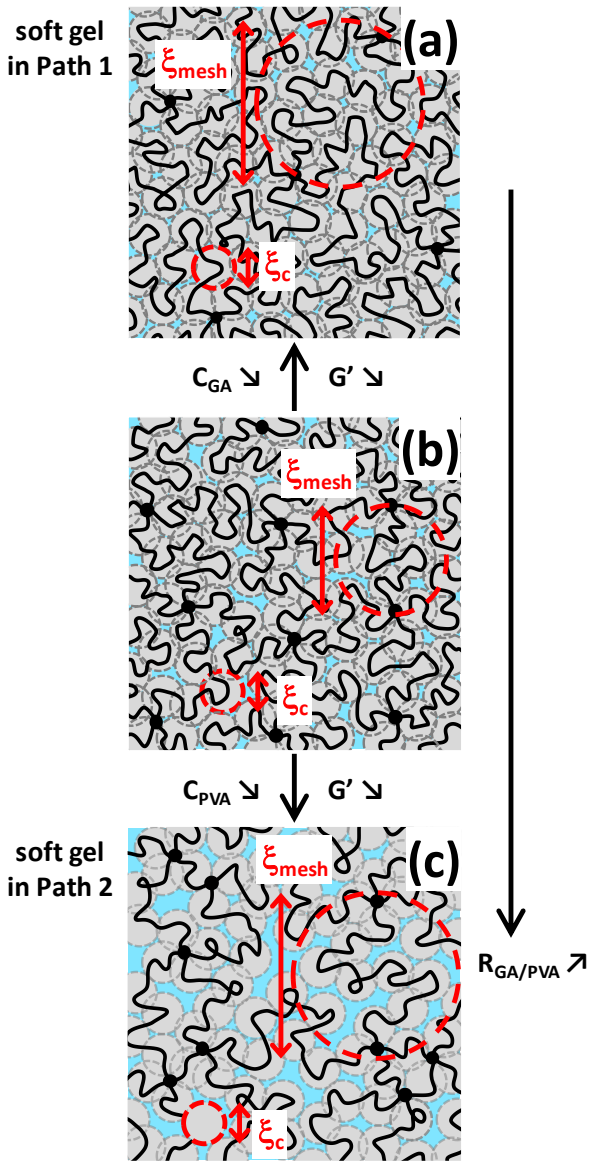

Figure 5. Proposed network structures of the gels from the two paths. (a) A first soft gel from Path 1 (C_{PVA} = 6.6 wt% and C_{GA} = 4.2 mM) where a relatively homogeneous network is proposed. (b) Reference gel found for both Path 1 and 2

(C_{PVA} = 6.6 wt% and C_{GA} = 7 mM). (c) Soft gel from Path 2 (C_{PVA} = 3.3 wt% and C_{GA} = 7 mM) is expected to have a more heterogeneous structure. ξ_c: correlation length estimated from light scattering, and ξ_{mesh}: mesh size of the network estimated from modulus.

Fracture Mechanics Studied by Puncture.

Modulus Measurements from Neo-Hookean Model

Figure 6a shows a schematic of the custom puncture setup. The loading force as a function of displacement or time can be recorded during the puncture process. **Figure 6b** shows a representative displacement profile of a needle insertion/retraction cycle. **Figure 6d** shows a representative puncture loading and unloading curves for a PVA hydrogel made from Path 1 with G' =800 Pa (C_{PVA} = 6.6 wt% and C_{GA} = 7 mM). The puncture force nonlinearly increases with displacement and sharply decreases when the needle tip breaks through the surface of the gel and fracture occurs. The values of critical puncture force F_c and critical displacement d_c are determined at the peak. After reversal during unloading, the force gradually decreases with decreasing displacement, reaching zero at a displacement close to d_c. In this indenter retraction process, the absolute value of negative force is much lower than that of the loading process, indicating that the friction force between the indenter and the gel is negligible in this system. In this work we will only focus on the loading curves up to the fracture point.

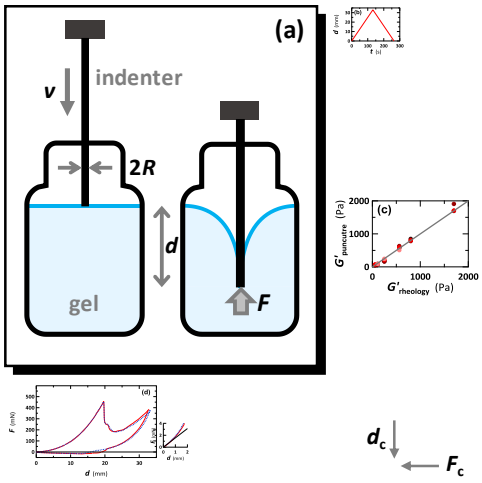

Figure 6. (a) Schematic of the puncture setup. (b) Typical indenter displacement profile. (c) Comparison of the elastic modulus of gels determined by puncture (from the linear regime, see the inset of Figure 6d) with those obtained by rheology (x axis). (d) Loading curves of a PVA hydrogel from Path 1 (C_{PVA} = 6.6 wt% and C_{GA} = 7 mM) with R = 0.23 mm. Two curves from two different samples made under the same conditions are shown (red solid curve and blue dashed curve). The gray solid line indicates F = 0. The critical force is defined as F_c and the critical displacement is defined as d_c. Inset: zoom-in of the force curves for linear regime to determine the modulus by fitting with the linear part of the Neo-Hookean model (gray solid line).

The Neo-Hookean model is employed here to describe the loading behavior of the puncture process,[18]

$$F = k'Ed^2 + k''ERd \qquad 3$$

where F is the puncture force, E is the Young's modulus of the material, d is the displacement of the indenter tip. k' is an empirical coefficient, and k'' is a constant depending on indenter tip geometry from Hertzian contact mechanics (for flat-end indenters). At a small indentation depth where the contact region $d \sim R$, the force curve can be fitted with the linear part of the Neo-Hookean model $F = \frac{8}{3}ERd$, as shown in the inset of **Figure 6d**. With the known k'' and needle radius, the shear modulus G is determined by assuming a Poisson's ratio v = 0.5 and $E = 2G(1+v)$ for incompressible gel samples. The value of G determined from the linear regime of the puncture test is compared with G' measured by linear rheology at 1 Hz. As shown in **Figure 6c**, the elastic moduli from the two measurement methods are comparable, indicating that the elastic modulus can be accurately measured from the small indentation conditions of the puncture process.

At large indentation depths the whole loading curve before the fracture point is fit to the Neo-Hookean model by setting k''= 8/3, and $k'E$ as a fitting parameter (red dashed curve in **Figure S5**). The fitting is not satisfactory for our system: though the curve captures the general features of the experimental force curve, it overestimates the force at the intermediate indentations and underestimates it at large indentations. The experimental data was fit with the Neo-Hookean model in its modified form,

$$\frac{F}{Ed} = k'd + k''R \qquad 3'$$

where k' is a fitting parameter and k'' = 8/3 (blue solid line in the inset of **Figure S5**). This fit demonstrates that up to intermediate indentation depth of about d < 7, the model fits well the experimental result, and that at large indentation depths the experiment force deviates from the

model giving larger values. We performed this fit for all the gels studied in this work and the value of k' is summarized in **Table S1**. The average value of k' is 0.27, which is very close to the literature value (0.26, for the acrylic copolymer gel with flat indenters).[17,18,28] This result suggests that the Neo-Hookean model describes well the indentation depth dependence of the puncture force before the strain hardening (blue solid line in **Figure S5**).

Non-Linear and Fracture Mechanics

The nonlinear response and fracture behavior of PVA hydrogels are characterized by the actual puncture process. **Figure 7** shows typical loading curves for gels from Path 1 and from Path 2 with a puncture needle radius of R = 0.23 mm. As expected, the force F and its critical value F_c increase with G' for gels from both paths, while the critical puncture displacement d_c displays a different modulus dependence. For the gels from Path 1, the value of d_c increases with decreasing modulus, and for the gels from Path 2, the trend seems more complex. In the geometry of a puncture, it is not possible to determine the fracture energy per unit area of the crack in the classical Griffith sense. However it is possible to estimate it globally by measuring the energy dissipated during the puncture process by integrating the hysteresis between the loading and unloading curves and normalizing it by the area of the created surface during the cracking process. Note however that it is often difficult to measure accurately the fracture surface because crack propagation is not controlled and is typically nonplanar in the puncture tests. In the rest of this paper, we analyze F_c and d_c to understand the fracture mechanism.

Figure 7. Puncture loading curve for gels from Path 1 (a) and from Path 2 (b). Needle radius, R = 0.23 mm.

The value of d_c is plotted as a function of modulus for different needle radius R for gels from both paths in **Figure 8a** and **8b**. For gels from Path 1 (**Figure 8a**), d_c is found to monotonously increase with decreasing modulus, and with increasing needle radius. The gels from Path 2 exhibit a more complex modulus and radius dependences as shown in **Figure 8b**. Notably, d_c for the softest gel is significantly lower than that for the gel from Path 1, which has a comparable modulus. With a decrease in modulus, d_c increases then decreases, and the amplitude of the decrease in d_c is more significant for higher R. The value of d_c is normalized by needle size R, and plotted as a function of the modulus in **Figure 8c** and **8d**. The curves of d_c/R for different

values of R do not superpose for both paths. The values of d_c/R could reach about 110 for the soft gels from Path 1. Fakhouri et al. reported that d_c is about 13 times R for acrylic triblock copolymer gels with moduli ranging from 2 to 13 kPa.[18] In our work we have much higher values of d_c/R, demonstrating distinct mechanics for these ultrasoft gels.

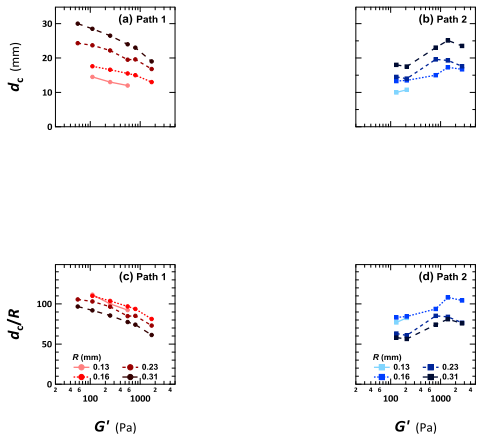

Figure 8. Critical puncture displacement d_c as a function of gel modulus G' for gels from Path 1 (a) and from Path 2 (b) with varied needle radius R. d_c normalized by R as a function of G' for gels from Path 1 (c) and from Path 2 (d).

In order to evaluate the modulus dependence of the critical puncture displacement normalized by the needle size, d_c/R, here we attempt to predict the trends of the stretch limit of the polymer chains λ_m and the stretch at break λ_b of the soft networks. In a dry polymer network containing n polymer chains per unit volume, the stretch limit of polymer chains, λ_m, can be expressed as [29]

$$\lambda_m = \frac{Nb}{\sqrt{N}b} = N^{1/2} \qquad 4$$

where N is the number of Kuhn monomers between two successive covalent cross-links, and b is the Kuhn monomer length. Nb and $\sqrt{N}b$ are the end-to-end distances of a polymer chain in the fully stretched state and in the relaxed state, respectively. The shear modulus (or elastic modulus) of the network in small strain, assuming the affine network model is [29]

$$G' = nkT \quad (5)$$

where k is the Boltzmann constant and T is the absolute temperature. Also, we have $Nn\nu = 1$, where ν is the volume of a Kuhn monomer. Since $N = 1/n\nu$ and $N \sim G'^{-1}$, we have

$$\lambda_m \sim G'^{-1/2} \quad (6)$$

The prediction of the stretch at break λ_b involves more assumptions and relies on the energy approach of fracture. According to the Lake-Thomas model describing the fracture of soft networks, the minimum fracture energy required to fracture an elastomer or a gel per unit area is

$$\Gamma = n\sqrt{N}bNU_f = nbN^{3/2}U_f \quad (7)$$

where $n\sqrt{N}b$ is the number of polymer strands that need to be broken per unit area of fracture surface, NU_f is the energy proposed by Lake and Thomas to fracture a single polymer strand, and U_f is the bond energy of the C-C bonds of a Kuhn monomer. Combining the above equations, the fracture energy Γ_0 of the hydrogel due to bond scission should scale as,[30,31]

$$\Gamma_0 \sim G'^{-1/2} \quad (8)$$

In the presence of a crack the energy release rate $\mathcal{G}$ is proportional to the elastic energy stored in the material per unit volume and scales with $G'\lambda^2$. At the fracture point of the soft network ($\lambda = \lambda_b$), by definition $\mathcal{G} = \Gamma_0$, therefore one would expect that at fracture $G'\lambda_b^2 \sim G'^{-1/2}$, and we have

$$\lambda_b \sim G'^{-3/4} \qquad 9$$

a stronger scaling than the one predicted by the stretching of a single linear chain (eq.4).[31] The question is then whether the fracture criterion of the soft gels in a puncture geometry is controlled by eqs 4 or 9. Based on Figures 8 and 11, d_c is weakly dependent on the modulus, i.e. the scaling exponent of d_c/R for the gel from Path 1 is about –0.1 and thus is much weaker than that of λ_m (for chains, –1/2) and of λ_b (for network, –3/4). This result suggests that the fracture point of the gels in puncture is neither controlled by the extensibility limit of individual polymer chains nor by a Lake-Thomas argument validated for simple cracks under extension.[32] As a consequence it can therefore clearly not be explained within the framework of the fracture of a homogeneously cross-linked gel.

The critical puncture force F_c is now characterized by varying both the modulus and needle radius. For the gels from both Path 1 and Path 2, F_c is found to increase with the gel modulus G' and R (**Figure 9a** and **9b**). Although the stress field is highly inhomogeneous spatially, it is reasonable to define a critical nominal stress σ_c as F_c normalized by the cross-sectional area of the needle, $\sigma_c = F_c/\pi R^2$. In **Figure 9c** and **9d**, the value of σ_c is plotted as a function of the modulus. The curves of σ_c for different radii seem to superpose well, although one can see a radius dependence in the high modulus range. This superposition, which is much better than that of d_c/R shown in Figure 8, suggests that the mechanism of fracture of gels from both paths is

controlled by the local stress (defined by the needle radius for a given force) and fracture presumably starts from a defect that is smaller than the needle size.[33]

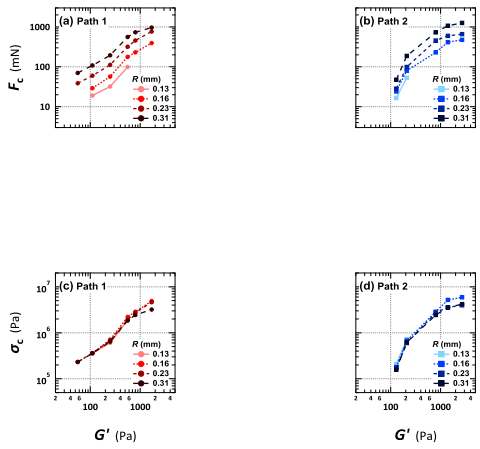

Figure 9. Critical puncture force F_c versus modulus for gels from Path 1 (a) and from Path 2 (b). Critical nominal stress σ_c versus modulus for gels from Path 1 (c) and from Path 2 (d).

Effects of Structural Heterogeneity and Elasto-Capillarity

The critical nominal stress σ_c is further analyzed by normalizing it with the modulus G'. This dimensionless quantity σ_c/G' is a characteristic of the resistance to fracture initiation of soft materials[18]. Since the needle size R, the characteristic length scale of the puncture tests, is comparable to the elasto-capillary length l_{ec} of the system studied, in order to evaluate a potential elasto-capillary effect on the puncture process, we plot σ_c/G' as a function of needle radius normalized by the elasto-capillary length, $R/l_{ec} = RG'/\gamma$ (**Figure 10**). This representation allows us to examine both the G' and R dependences. For the gels from Path 1 (**Figure 10a**), the value

of σ_c/G' varies between about 1700 and 5300. This result, the nominal stress surpassing the modulus by 3 orders of magnitude, is somehow surprising ($\sigma_c/G' \sim 150$ was previously reported for triblock polymers[18]), indicating the considerable fracture resistance of ultrasoft PVA hydrogels in the puncture geometry. σ_c/G' exhibits a universal trend, and it decreases with increasing R/l_{ec}. The gray dashed curve in **Figure 10a** is the result of a power-law fit with an exponent of –0.19. For the gels from Path 2 (**Figure 10b**), the value of σ_c/G' at low R/l_{ec} is about 1200 – 1900, much lower than that of the gels from Path 1 in the same range of R/l_{ec}. At R/l_{ec} higher than about 3, the value of σ_c/G' is comparable to that of the gels from Path 1.

From the obtained results, we cannot conclude that there is a clear effect of elasto-capillarity on the critical nominal stress of puncture. One would expect to have elasto-capillarity effects become important at $RG'/\gamma < 1$; however, no particular change in the trend is found for σ_c/G' for the gels from Path 1. For the gels from Path 2, the change in the trend at $RG'/\gamma \sim 3$ coincides with the increase in the heterogeneity of the soft gels shown by light scattering experiments. This result could be explained by the fracture process zone model, suggesting that the fracture mechanism of the current system is stress-limited and the energy criterion, including the elastocapillary effect, does not determine the fracture point. Another possible mechanism is that the new surface created by fracture in the puncture geometry might be an interface between the hydrogel and water appearing by poroelasticity, but not an interface between the hydrogel and air. In this case the true elastocapillary length would be much smaller than our estimation.

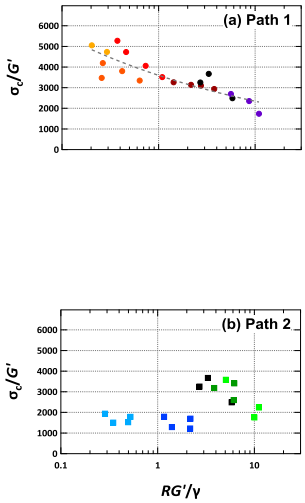

Figure 10. Critical nominal stress normalized by the modulus, σ_c/G', as a function of indenter radius R normalized by elasto-capillary length γ/G' for gels from Path 1 (a) and Path 2 (b).

The normalized critical displacement d_c/R is plotted as a function of RG'/γ in **Figure 11**. For the gels from Path 1 (**Figure 11a**), all the data points collapse on a master curve, exhibiting a power-law behavior with an exponent of –0.11 (gray dashed curve). We do not find changes in trends at $RG'/\gamma \sim 1$, suggesting again that elasto-capillarity does not noticeably influence the fracture mechanism of this system in the puncture geometry. The data for the gels from Path 2 (**Figure11b**) are more scattered than those for the gels from Path 1 and no clear trend can be distinguished. When the two paths are compared at low RG'/γ, i.e., for the softer gels, the value of d_c/R for the gels from Path 2 is distinctly lower than that of the gel from Path 1.

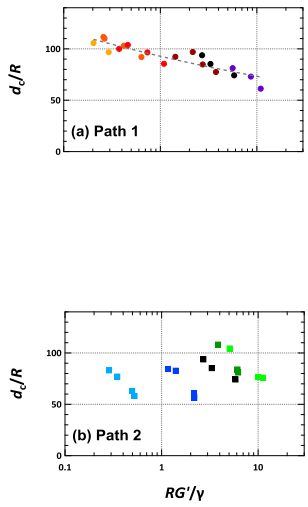

Figure 11. Critical displacement normalized by radius, d_c/R, as a function of indenter radius R normalized by elasto-capillary length γ/G' for gels from Path 1 (a) and Path 2 (b).

Based on the analysis of the structural information via light scattering, we attribute the difference in fracture resistance of the two gel families to their differences in structural heterogeneity, related to the heterogeneous spatial distribution of permanent cross-links leading to the distribution of network strand size. Contrary to the linear modulus, the fracture resistance of the polymer networks under large deformation is largely affected by the structural heterogeneity originating from the wide distribution in the network strand length. The heterogeneous network structure in length and conformation of strands and in topology, leads to a very heterogeneous distribution of forces on the chemical bonds. Clusters of overstressed strands or cross-linkers lead to crack initiation in these regions resulting in the macroscopic fracture. As demonstrated by

light scattering measurements, the soft gels from Path 2 have a more heterogeneous structure than the soft gels from Path 1, which have a comparable modulus. As illustrated in **Figure 12**, in the soft gel from Path 1 the network could sustain large deformations by evenly distributing the applied stress and delaying crack nucleation involving chain scission. In the soft gels from Path 2, the externally applied stress tends to concentrate on localized overstressed chains, nucleate larger defects, and result in the catastrophic failure of the material. Consequently, we attain a lower critical deformation and fracture resistance of the inhomogeneous gel when compared to the homogeneous one.

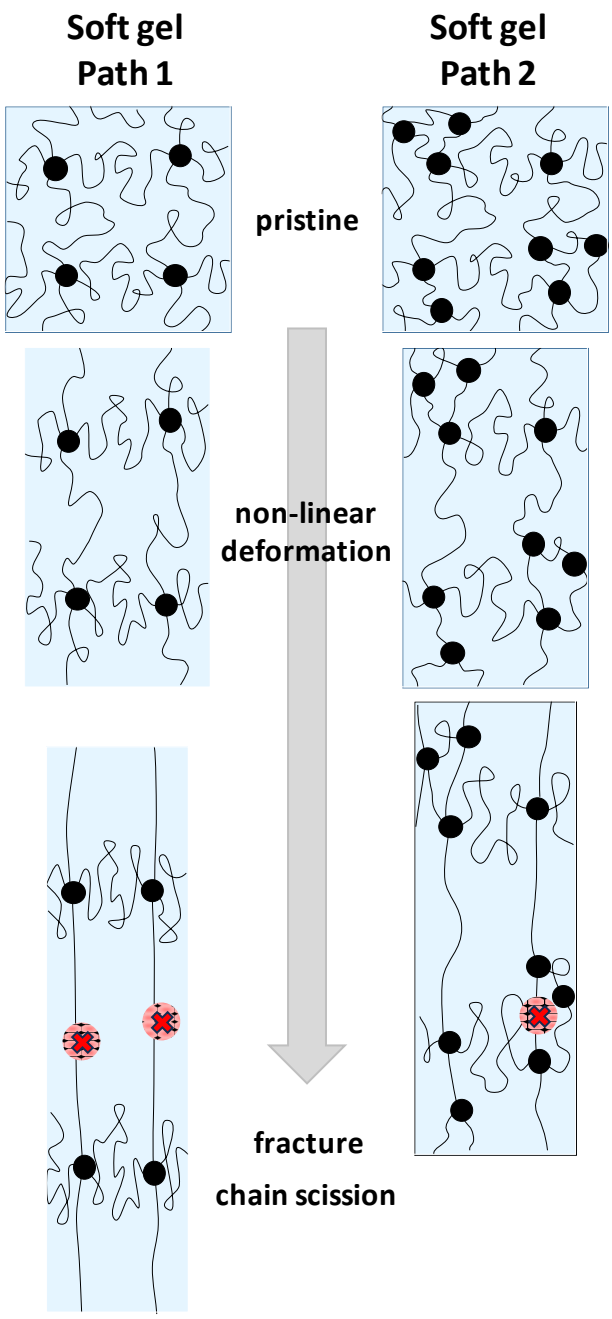

Figure 12. Schematic of network evolution under the needle tip prior to indentation, at large strain deformation, and at the point of fracture. Gels from Path 2 present high structure inhomogeneity compared to gels from Path 1 and sustain less large deformation when polymer chains cannot behave cooperatively to applied stress.

CONCLUSIONS

PVA hydrogels chemically cross-linked by GA were used as a model system to investigate the fracture properties of soft solids by puncture tests. By tuning the gel modulus and flat indenter radius (130 – 310 μm), the fracture properties of the ultrasoft gels at a length scale comparable to the elasto-capillary length (19 – 911 μm) were studied. Synthesizing ultrasoft hydrogels by decreasing polymer and/or cross-linker concentrations approaching the percolation limits could lead to different types of structural heterogeneities, which could strongly affect non-linear mechanical properties. We prepared PVA hydrogels having moduli ranging from 56 to 2700 Pa, with two synthetic paths (Path 1: constant PVA concentration and varied GA concentration, Path 2: varied PVA concentration and constant GA concentration). The structural heterogeneities of the gels were evaluated by light scattering. Both the amplitude of the long time plateau and the unfluctuating component of the autocorrelation function of the scattered light were used as characteristics of the degree of heterogeneity, and we found that the soft gels from Path 2, close to the site percolation limit, exhibit pronounced network heterogeneity, compared to the gels from Path 1 having a comparable modulus. The fracture properties of the PVA hydrogels were characterized by the critical nominal puncture force and critical displacement normalized by the indenter cross-section and by the indenter radius respectively. These two characteristic values exhibit a universal behavior as a function of the indenter radius normalized by the elasto-capillary length, for the gels from Path 1, which have a less heterogeneous network structure than those from Path 2. The soft gels from Path 2, having a more pronounced network heterogeneity, exhibit a lower critical nominal stress and critical deformation than those from Path 1, which have a comparable modulus. This work reveals the importance of the structural

heterogeneity of soft gels on the nonlinear mechanical properties. We do not, however, find clear evidence of elasto-capillarity effects on the fracture properties in this geometry. A further systematic study with soft gels on an expanded length scale would be necessary for a more quantitative argument. Different characteristic lengths should be more accurately estimated, including the elastocapillary length (with the surface tension of the hydrogels), and the size of the fracture process zone (from the fracture energy measured by another technique).

ASSOCIATED CONTENT

The Supporting Information is available free of charge at http://pubs.acs.org/ .

Supporting figures (S1 – S5), and supporting table (S1).

CORRESPONDING AUTHORS

Tetsuharu Narita − Laboratoire Sciences et Ingénierie de la Matière Molle, CNRS UMR 7615, ESPCI Paris, Sorbonne Université, PSL Université, 75005 Paris, France.

orcid.org/0000-0002-2061-1357

Email: tetsuharu.tarita@espci.fr.

Costantino Creton − Laboratoire Sciences et Ingénierie de la Matiere` Molle, CNRS UMR 7615, ESPCI Paris, Sorbonne Université, PSL Université, 75005 Paris, France;

orcid.org/0000-0002-0177-9680;

Email: costantino.creton@espci.fr.

AUTHOR INFORMATION

Yuanyuan Wei − Laboratoire Sciences et Ingénierie de la Matiere` Molle, CNRS UMR 7615, ESPCI Paris, Sorbonne Université, PSL Université, 75005 Paris, France;

orcid.org/0000-0001-7577-8122

Donghao Zhao − Laboratoire Sciences et Ingénierie de la Matiere` Molle, CNRS UMR 7615, ESPCI Paris, Sorbonne Université, PSL Université, 75005 Paris, France;

https://orcid.org/0000-0001-8791-7054

FUNDING SOURCES

The authors declare no competing financial interest.

ACKNOWLEDGMENT

Yuanyuan Wei and Donghao Zhao have benefited from a scholarship from the Chinese Scholarship Council. This project has received funding from the European Research Council (ERC) under the European Union's 2020 Research and Innovation Program (grant agreement no. 695351, CHEMECH). This project is partly supported by the Agence Nationale de Recherche (GelWet, ANR-17-CE30-0016). The authors thank Guylaine Ducouret from SIMM Lab for her help in rheology experiments.

REFERENCES

1. Lee, K. Y.; Mooney, D. J., Hydrogels for tissue engineering. *Chem. Rev.* **2001,** *101* (7), 1869-1880.

2. Livne, A.; Ben-David, O.; Fineberg, J., Oscillations in rapid fracture. *Phys. Rev. Lett.* **2007,** *98* (12), 124301.

3. Livne, A.; Cohen, G.; Fineberg, J., Universality and hysteretic dynamics in rapid fracture. *Phys. Rev. Lett.* **2005,** *94* (22), 224301.

4. Bonn, D.; Kellay, H.; Prochnow, M.; Ben-Djemiaa, K.; Meunier, J., Delayed fracture of an inhomogeneous soft solid. *Science* **1998,** *280* (5361), 265-267.

5. Kong, H. J.; Wong, E.; Mooney, D. J., Independent control of rigidity and toughness of polymeric hydrogels. *Macromolecules* **2003,** *36* (12), 4582-4588.

6. Gong, J. P.; Katsuyama, Y.; Kurokawa, T.; Osada, Y., Double- network hydrogels with extremely high mechanical strength. *Adv. Mater.* **2003,** *15* (14), 1155-1158.

7. Creton, C., 50th anniversary perspective: Networks and gels: Soft but dynamic and tough. *Macromolecules* **2017,** *50* (21), 8297-8316.

8. Ducrot, E.; Chen, Y.; Bulters, M.; Sijbesma, R. P.; Creton, C., Toughening elastomers with sacrificial bonds and watching them break. *Science* **2014,** *344* (6180), 186-189.

9. Abolhassani, N.; Patel, R.; Moallem, M., Needle insertion into soft tissue: A survey. *Med. Eng. Phys.* **2007,** *29* (4), 413-431.

10. McCreery, G. L.; Trejos, A. L.; Naish, M. D.; Patel, R. V.; Malthaner, R. A., Feasibility of locating tumours in lung via kinaesthetic feedback. *Int. J. Med. Robot. Comput. Assist. Surg.* **2008,** *4* (1), 58-68.

11. Jagota, A.; Paretkar, D.; Ghatak, A., Surface-tension-induced flattening of a nearly plane elastic solid. *Phys. Rev. E* **2012,** *85* (5), 051602.

12. Hui, C.; Jagota, A.; Lin, Y.-Y.; Kramer, E., Constraints on microcontact printing imposed by stamp deformation. *Langmuir* **2002,** *18* (4), 1394-1407.

13. Liu, T.; Long, R.; Hui, C.-Y., The energy release rate of a pressurized crack in soft elastic materials: effects of surface tension and large deformation. *Soft Matter* **2014,** *10* (39), 7723-7729.

14. Hui, C.-Y.; Liu, T.; Schwaab, M.-E., How does surface tension affect energy release rate of cracks loaded in Mode I? *Extreme Mech. Lett.* **2016,** *6*, 31-36.

15. Xu, X.; Jagota, A.; Peng, S.; Luo, D.; Wu, M.; Hui, C.-Y., Gravity and surface tension effects on the shape change of soft materials. *Langmuir* **2013,** *29* (27), 8665-8674.

16. Wei, Y.; Ju, J.; Creton, C.; Narita, T., Unexpected Fracture Behavior of Ultrasoft Associative Hydrogels Due to Strain-Induced Crystallization. *ACS Macro Lett.* **2023,** *12*, 1106-1111.

17. Rattan, S.; Crosby, A. J., Effect of polymer volume fraction on fracture initiation in soft gels at small length scales. *ACS Macro Lett.* **2019,** *8* (5), 492-498.

18. Fakhouri, S.; Hutchens, S. B.; Crosby, A. J., Puncture mechanics of soft solids. *Soft Matter* **2015,** *11* (23), 4723-4730.

19. Rattan, S.; Li, L.; Lau, H. K.; Crosby, A. J.; Kiick, K. L., Micromechanical characterization of soft, biopolymeric hydrogels: stiffness, resilience, and failure. *Soft Matter* **2018,** *14* (18), 3478-3489.

20. Shibayama, M.; Norisuye, T., Gel formation analyses by dynamic light scattering. *Bull. Chem. Soc. Jpn.* **2002,** *75* (4), 641-659.

21. Webber, R. E.; Creton, C.; Brown, H. R.; Gong, J. P., Large strain hysteresis and mullins effect of tough double-network hydrogels. *Macromolecules* **2007,** *40* (8), 2919-2927.

22. Fuse, C.; Okabe, S.; Sugihara, S.; Aoshima, S.; Shibayama, M., Water-induced self-assembling of solvent-sensitive block copolymer. *Macromolecules* **2004,** *37* (20), 7791-7798.

23. Shibayama, M., Small-angle neutron scattering on polymer gels: phase behavior, inhomogeneities and deformation mechanisms. *Polym. J.* **2011,** *43* (1), 18-34.

24. Sato, T.; Okaya, T., Physical and Surface Properties of Aqueous Solutions of Polyvinyl Alcohols Having an n-Alkylthio End Group. *J. Appl. Polym. Sci* **1992**, 46, 641 – 647.

25. Nakamae, M.; Yuki, K.; Sato, T.; Maruyama, H., Preparation of polymer emulsions using a poly(vinyl alcohol) as protective colloid, *Colloids Surf. A* **1999**, 153, 367 – 372.

26. Narita, T.; Mayumi, K.; Ducouret, G.; Hebraud, P., Viscoelastic properties of poly (vinyl alcohol) hydrogels having permanent and transient cross-links studied by microrheology, classical rheometry, and dynamic light scattering. *Macromolecules* **2013,** *46* (10), 4174-4183.

27. Pusey, P.N.; Van Hegen, W., Dynamic light scattering by non-ergodic media. *Physica A* **1989**, *157*(2), 705 – 741.

28. Rattan, S.; Crosby, A. J., Effect of far-field compliance on local failure dynamics of soft solids. *Extreme Mech. Lett.* **2018,** *24*, 14-20.

29. Rubinstein, M.; Colby, R., Oxford University Press; New York: 2003. *Polymer Physics.*

30. Lake, G.; Thomas, A., The strength of highly elastic materials. *Proc. R. Soc. A Math. Phys. Sci.* **1967,** *300* (1460), 108-119.

31. Creton, C.; Ciccotti, M., Fracture and adhesion of soft materials: a review. *Rep. Prog. Phys.* **2016,** *79* (4), 046601.

32. Akagi, Y.; Sakurai, H.; Gong, J.-P.; Chung, Y.-I.; Sakai, T., Fracture energy of polymer gels with controlled network structures. *J. Chem. Phys*. **2013**, *139*(14): 144905.

33. In the context of a fracture process zone model, a crack can propagate, when both local stress (to break chemical bonds) and energy (to do the work to separate new interfaces) reach their critical value. Our result suggests that the fracture mechanism of this system is stress-limited, or the fracture occurs when the stress reaches the critical value and there is already

sufficient strain energy available in the surrounding volume. In this condition the size of the fracture process zone should be smaller than the needle radius.